



Pupillary Dynamics Link Spontaneous and Task-Evoked Activations Recorded Directly from Human Insula

 Aaron Kucyi¹ and  Josef Parvizi²

¹Department of Psychology, Northeastern University, Boston, Massachusetts 02115, and ²Department of Neurology & Neurological Sciences, Stanford University, Stanford, California 94304

Spontaneous activations within neuronal populations can emerge similarly to “task-evoked” activations elicited during cognitive performance or sensory stimulation. We hypothesized that spontaneous activations within a given brain region have comparable functional and physiological properties to task-evoked activations. Using human intracranial EEG with concurrent pupillometry in 3 subjects (2 males, 1 female), we localized neuronal populations in the dorsal anterior insular cortex that showed task-evoked activations correlating positively with the magnitude of pupil dilation during a continuous performance task. The pupillary response peaks lagged behind insular activations by several hundreds of milliseconds. We then detected spontaneous activations, within the same neuronal populations of insular cortex, that emerged intermittently during a wakeful “resting state” and that had comparable electrophysiological properties (magnitude, duration, and spectral signature) to task-evoked activations. Critically, similar to task-evoked activations, spontaneous activations systematically preceded phasic pupil dilations with a strikingly similar temporal profile. Our findings suggest similar neurophysiological profiles between spontaneous and task-evoked activations in the human insula and support a clear link between these activations and autonomic functions measured by dynamics of pupillary dilation.

Key words: arousal; attention; intracranial EEG; pupillometry; resting state; sympathetic

Significance Statement

Most of our knowledge about activations in the human brain is derived from studies of responses to external events and experimental conditions (i.e., “task-evoked” activations). We obtained direct neural recordings from electrodes implanted in human subjects and showed that activations emerge spontaneously and have strong similarities to task-evoked activations (e.g., magnitude, temporal profile) within the same populations of neurons. Within the dorsal anterior insula, a brain region implicated in salience processing and alertness, activations that are either spontaneous or task-evoked are coupled with brief dilations of the pupil. Our findings underscore how spontaneous brain activity, a major current focus of human neuroimaging studies aimed at developing biomarkers of disease, is relevant to ongoing physiological and possibly self-generated mental processes.

Introduction

Spontaneous activity within and across distinct neuronal populations has been the basis for studies of intrinsic functional networks within the human brain (Fox and Raichle, 2007; Nir et al.,

2008; Kucyi et al., 2018b). In functional neuroimaging and electrophysiological data, intrinsic networks, based on correlated spontaneous activity between brain regions, show similar spatial distributions as activations evoked explicitly during cognitive task performance (Smith et al., 2009; Mennes et al., 2010; Foster et al., 2015; Tavor et al., 2016). Importantly, recent functional neuroimaging studies suggest that brief, transient, spontaneous activations may contribute substantially to the observed task-like distributions of intrinsic networks (X. Liu and Duyn, 2013; Karahanoglu and Van De Ville, 2015). However, the spatiotemporal profile of these brief, spontaneous activations and their relationship with task-evoked activations have been almost solely inferred from neuroimaging data that are limited in temporal resolution and signal-to-noise ratio, making it difficult, if not impossible, to make inferences about the profiles and physiological relevance of such activations at the neuronal population level.

Received Feb. 23, 2020; revised Apr. 29, 2020; accepted May 18, 2020.

Author contributions: A.K. and J.P. designed research; A.K. and J.P. performed research; A.K. analyzed data; A.K. wrote the first draft of the paper; A.K. and J.P. edited the paper; A.K. and J.P. wrote the paper.

This work was supported by National Institute of Neurological Disorders and Stroke Grant R01NS078396, National Institute of Mental Health Grant 1R01MH109954-01, and National Science Foundation Grant BCS1358907 to J.P. A.K. was supported by Canadian Institutes of Health Research Banting Fellowship. We thank Clara Sava-Segal, Jennifer Yih, Lucie Petetin, Andero Uusberg, and Michael Esterman for assistance with data collection and technical support; and Nikolai Axmacher and James Mac Shine for feedback and suggestions on analysis approaches.

The authors declare no competing financial interests.

Correspondence should be addressed to Josef Parvizi at jparvizi@stanford.edu.

<https://doi.org/10.1523/JNEUROSCI.0435-20.2020>

Copyright © 2020 the authors

Here we aim to address this shortcoming using human intracranial EEG (iEEG), which offers a sensitive method to study neuronal population activity with high temporal resolution (Parvizi and Kastner, 2018). Moreover, to characterize the functional significance of spontaneous activity, we uniquely combined iEEG with pupillometry. Intrinsic fluctuations of pupil size are known to be a sensitive marker of fluctuations in autonomic arousal (Murphy et al., 2014; Reimer et al., 2014, 2016; McGinley et al., 2015; Yellin et al., 2015; Joshi et al., 2016; Schneider et al., 2016; Shine et al., 2016; Mathôt, 2018; Stitt et al., 2018; Stringer et al., 2019). Electrophysiological studies in animal models suggest that spontaneous, phasic pupil dilations are associated with preceding neuronal firing in the brainstem (locus ceruleus), cingulate cortex, and corticopetal noradrenergic and cholinergic projections (Reimer et al., 2014, 2016; Joshi et al., 2016). Moreover, human resting-state fMRI studies have linked spontaneous pupil fluctuations with slow hemodynamic activity in large-scale cortical networks, including the salience network (Murphy et al., 2014; Yellin et al., 2015; Schneider et al., 2016; Breeden et al., 2017).

A key region that is within the salience network, and that may be well positioned to coordinate cortical activity with ascending brainstem systems implicated in alertness, is the dorsal anterior insula (daIC) (Seeley et al., 2007; Menon and Uddin, 2010; Uddin, 2015). The daIC is activated across an extensive variety of task conditions involving both exteroceptive attention and awareness of internal bodily sensations (Craig, 2009). A possible parsimonious explanation for daIC engagement is a domain-general role in the detection of behaviorally relevant, salient stimuli and sensations (Menon and Uddin, 2010). Interestingly, the daIC shows a similar response profile to the pupil across various conditions. Both are sensitive to arousal (Aston-Jones and Cohen, 2005; Young et al., 2017), stimulus salience (Downar et al., 2002; Wang and Munoz, 2014), error monitoring (Dosenbach et al., 2006; Smallwood et al., 2011; Fortenbaugh et al., 2018), and neuromodulatory activity within the noradrenergic system (Hermans et al., 2011; Zerbi et al., 2019). It remains unknown, however, whether phasic pupil dilation is consistently time-locked to spontaneous daIC activations that have similar properties to task-evoked activations.

We recently developed an iEEG paradigm that allows reliable functional localization of task-evoked neuronal population activations within the salience network, including the insula (Kucyi et al., 2020). Here we report novel and independent analyses within a subset of the subjects from our past work who had extensive electrode coverage within the insula and who underwent pupillometry during iEEG recordings. We compared spontaneous and task-evoked activations in the daIC and examined the relationship between “task-like” spontaneous activation within discrete daIC neuronal populations and temporal coupling to pupil dilations.

Materials and Methods

Subjects

Three human subjects (S1–S3, 1 female and 2 males) who were undergoing neurosurgical treatment for refractory focal epilepsy at Stanford University Medical Center were included in this study (for demographic and epilepsy details, see Table 1). All subjects were right-handed. Depth electrodes were implanted stereotactically within both hemispheres for invasive monitoring of epileptic activity over the course of 5–10 d. In all subjects, ictal discharge onsets were not found in the insular cortex. The subjects were part of a larger cohort that participated in some of the procedures described herein and were selected for this study based on the following inclusion criteria: (1) performed at least four 6 min runs of the

Gradual-Onset Continuous Performance Task (GradCPT) with pupillometry; (2) performed at least 15 min of wakeful rest (visual fixation) with pupillometry; and (3) had electrodes implanted within the daIC. Distinct analyses of the iEEG (but not pupil) data were reported previously (Kucyi et al., 2020). Subjects provided verbal and written consent to participate in research. The Stanford Institutional Review Board approved all procedures described herein. All described analyses and statistical procedures were performed within individuals, and individual subjects were thus treated as replication datasets.

Experimental design and statistical tests

Intracranial EEG data acquisition. Depth electrode placement was decided based on clinical evaluation for resective surgery. Depth electrode contacts (Ad-Tech Medical Instrument) had 0.86 mm diameter and 2.29 mm height with interelectrode spacing of 5–10 mm. Electrophysiological data were recorded with a Nihon Kohden clinical monitoring system with a sampling rate of 1000 Hz and a bandpass filter of 1.6–300 Hz. The iEEG signals were referenced to the most electrographically silent channel during recording. The number of electrodes within insular cortex and precise locations varied across subjects (see Fig. 1c).

All recordings were performed at bedside at the patient’s private clinical suite. During task performance and visual fixation sessions, stimuli were presented on a laptop running Windows 10 Pro, with the screen positioned ~70 cm from the patients’ eyes at chest level. We used Psychophysics Toolbox (Brainard, 1997) in MATLAB R2016b (The MathWorks) to present all stimuli. To align the onset times of recording runs and presented stimuli with iEEG data, we used an RTBox device (Li et al., 2010) that sent transistor-transistor logic pulses to an empty (DC) channel on the EEG montage.

Pupillometry. Pupil diameter was recorded with a SensoMotoric Instruments (Teltow) Remote Eye Tracking Device (RED250mobile) and iView software that interfaced with MATLAB. Eye tracking data were acquired with an infrared-light-sensitive video camera (250 Hz sampling rate) attached via a magnet to the area below the laptop monitor. Before each experimental run, subjects performed a 5 point calibration. Pupil diameter was recorded from the right eye in millimeter units with four decimal places. Within each run of pupillometry recording, the lighting in the room was kept dim and was not explicitly changed.

Continuous task performance. Subjects performed between four and eight 6 min runs of the GradCPT (Esterman et al., 2013) (some runs with and some without pupillometry). The number of runs obtained varied, depending on available time for research testing in the clinical environment (Table 1). Task runs were completed in multiple sessions when necessary.

During the GradCPT, grayscale images of cities (nontarget trials) and mountains (target trials) from the SUN database (Xiao et al., 2016), all luminance-matched (using the SHINE toolbox) (Willenbockel et al., 2010), were presented continuously. The images appeared within round frames over a white background and gradually transitioned from one to another, with each transition lasting 800 ms. Linear pixel-by-pixel interpolation was used for each image, with coherence peaking at 400 ms post-trial onset. After peaking, the image began to fade out to minimum coherence (800 ms post-trial onset). The first and last images of each run transitioned from and to, respectively, a blurred mask image (same size as other stimuli). There were 10 unique images of city and mountain scenes each. The order of trials was randomized (uniquely for each run) with a biased presentation rate of 10% mountains and 90% cities (the same scene never repeated on consecutive trials).

Participants were instructed to press the space bar key on the laptop when they noticed a city scene appearing that was distinct from the prior trial and to withhold their response when infrequent mountain stimuli were appearing. Each run began with a 20 s baseline period where the subject was asked to get ready. Before the first run, subjects completed 30 s of practice to get oriented to the task. Subjects were instructed to perform their best and to keep going, even when they noticed that they had made an error.

We used a previously described iterative algorithm (Esterman et al., 2013) to assign key presses to trials (relative to the beginning of each image transition). If the reaction time (RT) was before 70% image

Table 1. Subject demographics, disease characteristics, sessions performed, and behavioral performance^a

	S1	S2	S3
Age (yr)	31	19	49
Sex	M	F	M
Epilepsy duration (yr)	7	5	23
Sites showing epileptic activity (ictal or interictal)	Left anterior temporal lobe, left hippocampus, right hippocampus	Left lateral temporal lobe	Left medial posterior temporal lobe
No. of GradCPT runs (no. with pupillometry)	8 (4)	8 (6)	4 (4)
GradCPT mean RT (correct commissions; mean \pm SD, s)	0.76 \pm 0.18	0.71 \pm 0.19	0.84 \pm 0.17
GradCPT error rate (omission/commission)	0.09%/56.5%	1.7%/35.8%	2.9%/16.8%
No. of rest runs (total duration, min)	3 (17.3)	5 (32.2)	5 (29.4)
MNI coordinates of peak-responsive insula electrodes	$x = -31$ $y = 14$ $z = 11$	$x = -30$ $y = 25$ $z = 4$	$x = -31$ $y = 21$ $z = 7$

^aOmission error (failed button press for nontarget stimulus) and commission error (button press for target stimulus) rates are based on the mean across runs.

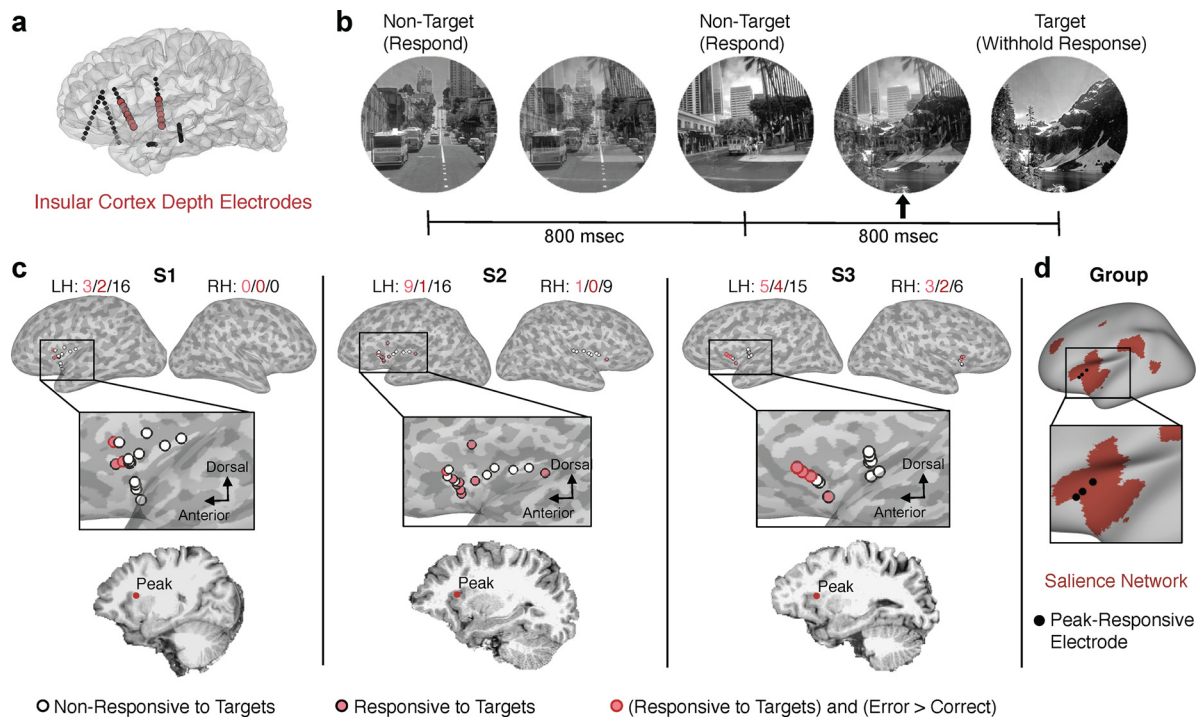


Figure 1. Task-evoked insula and pupil responses to target stimuli in the GradCPT. **a**, Depth probes with electrodes implanted in the insula (red) are illustrated in an example subject. **b**, The GradCPT paradigm. **c**, Locations of insula electrodes in 3 subjects are shown on the inflated cortical surface. Electrodes were classified into those showing no significant HFB response to GradCPT target relative to nontarget stimuli (white fill, black outline), a significant HFB increased response to target relative to nontarget stimuli (pink fill), and a significant HFB increased response for target trials with correct compared with incorrect behavioral responses (red outline) (Monte Carlo $p < 0.05$, cluster-based permutation test corrected for number of insula electrodes within subject). The location of the electrode with strongest HFB response within each subject is shown on a 2D sagittal slice. **d**, Locations of peak-responsive insula electrodes within each subject displayed on the inflated *fsaverage* cortical surface. Red represents the salience network, based on the fMRI-based Yeo atlas of seven cortical networks.

coherence for the current trial, or after 40% coherence on the following trial, the assignment was made as follows: (1) If there was no response on the previous or current trial, the current trial was assigned; (2) if both trials before and after the current trial had no responses, the trial closest in time was assigned (excluding cases where this trial was a mountain); and (3) if the above criteria led to multiple presses that could be assigned to a given trial, the fastest RT was assigned to the trial. Based on these criteria, trials were assigned to four categories: (1) correct commission (response to city), (2) omission error (no response to city), (3) correct omission (no response to mountain), and (4) commission error (response to mountain).

Resting-state visual fixation. As with GradCPT performance, the number of resting-state runs with pupillometry varied based on available

research testing time, and runs were completed in multiple sessions when necessary. Run duration varied between 5.4 and 7.8 min. The number of runs obtained varied across subjects, with total durations ranging from 17.3 to 32.2 min (Table 1). During resting-state runs, a white cross was displayed over a dark background. Participants were instructed to maintain their focus on the cross for the duration of the run but to otherwise relax and not think of anything in particular.

iEEG data preprocessing. Preprocessing of iEEG data was conducted within each run using a combination of SPM12 (Kiebel and Friston, 2004), Fieldtrip (Oostenveld et al., 2011), and custom MATLAB code, as described previously (Kucyi et al., 2018b, 2020). Task recordings were clipped such that only pretask baseline and task performance periods were retained. Notch filtering was applied to attenuate powerline noise

using a zero-phase, third-order, Butterworth filter with band stops between 57–63, 117–123, and 177–183 Hz. The signal from each channel was then rereferenced to the common average of all channels. For this rereferencing, the following types of channels were excluded from the common average: (1) noted by a neurologist to be within seizure foci; (2) had a variance greater or lesser than 5 times the median variance across all channels; (3) had 3 times the median number of spikes ($100\ \mu\text{V}$ changes between successive samples) across all channels; and (4) noted as clear outliers when inspecting the power spectra (e.g., not showing a typical $1/f$ curve). The rereferenced data were submitted to time-frequency decomposition with a Morlet wavelet transform (five cycles) applied to the range of 1–170 Hz (log-spaced, resulting in 38 distinct frequencies). The power amplitude estimates were then normalized within each frequency band via conversion to decibel units (i.e., multiplied by $10 \times \log_{10}$) and then subtracting out the mean of the log signal across the whole run. The power amplitude estimates were then averaged within the θ (4–8 Hz), α (8–12 Hz), β_1 (13–29 Hz), β_2 (30–39 Hz), γ (40–70 Hz), and high-frequency broadband (HFB) range (70–170 Hz) (Kucyi et al., 2018b). For analyses involving comparisons between iEEG and pupil diameter, we downsampled the HFB signal to 250 Hz.

Anatomical localization of electrodes. Subjects underwent a preoperative T1-weighted structural MRI (256×256 matrix, 160 slices, $0.94 \times 0.94 \times 1.00$ mm voxels, 240 mm FOV, 13 degree flip angle, 9.63 ms TR, and 3.88 ms TE). Following electrode implantation, a CT scan was obtained. We used the iElvis pipeline (Groppe et al., 2017) to anatomically localize electrode sites. First, we processed the T1 scan and performed surface reconstruction using Freesurfer v6.0.0 (*recon-all* command) (Fischl et al., 1999). We then performed alignment between the CT and T1 scans using a rigid transformation (6 df, affine mapping). Finally, using the T1-registered CT image, we manually labeled electrodes based on high-intensity voxels within BioImage Suite software (Papademetris et al., 2006) and obtained electrode coordinates via iElvis in 3D volumetric space. To visualize multiple electrodes within the insula at once, we mapped these coordinates to the nearest vertex location on the inflated cortical surface. To assess the correspondence between electrode locations and intrinsic networks described in the neuroimaging literature, we registered the electrode coordinates from individual to MNI305 space, and we overlaid the salience network derived from a population-level atlas of seven networks on the *fsaverage* cortical surface (Yeo et al., 2011).

Pupil data preprocessing. Within each run, we normalized the pupil diameter time series to z scores (subtracted out mean, then divided by SD). We interpolated missing values (e.g., because of blinks) using a spring metaphor (MATLAB function: *inpaint_nans.m*) to maintain smoothness of the time series. For analyses of pupil responses aligned to either task events (target and nontarget onsets) or iEEG events, we epoched the pupil time series around each event of interest with a -0.8 to 3 s window relative to event onset. We then rejected pupil epochs that were deemed to be of insufficient data quality based on the following criteria: (1) contained >1 s of consecutive samples within the raw data with missing values; or (2) had a mean overall z score of $>|2.5|$. For retained epochs, we performed baseline correction of the pupil diameter by subtracting out the mean value within the preevent window (-0.8 to 0 s). This baseline normalization procedure both enabled analysis of event-related relative changes in pupil diameter and accounted for possible drift in mean pupil diameter over time (i.e., across distinct epochs) (Mathôt, 2018). Finally, we applied smoothing with a 150 ms Gaussian kernel (selected to provide comparable results with those reported previously) (Joshi et al., 2016).

Task-evoked iEEG and pupil responses. Task-evoked iEEG responses were analyzed based on the HFB signal. For this analysis, the HFB signal was smoothed with a 150 ms Gaussian kernel (matching the pupil smoothing). Epochs from -0.8 to 3 s relative to trial onset were then obtained surrounding three types of trials: correct omissions, commission errors, and correct commissions. Target trials that were preceded by other target trials were excluded from analysis. Correct commission trials were considered as the baseline trial type because a significant HFB response was not expected (Kucyi et al., 2020). As the number of correct commissions was always larger than that for other categories, we took a

random subsample within each run such that the numbers of correct commissions were matched with the number of correct omissions or commission errors (whichever had more trials) before statistical procedures.

To assess significance of iEEG and pupil responses during the three different trial types, we performed cluster-based permutation tests (Maris and Oostenveld, 2007) within subjects. The tests were conducted for three contrasts: (1) correct omissions versus correct commissions, (2) correct omissions versus commission errors, and (3) commission errors versus correct omissions. For iEEG, significance was assessed within a 0 to 2 s window relative to trial onset. Given that pupil responses can be relatively slower and prolonged (Mathôt, 2018), a 0.3 to 3 s window was used. For each time point, we compared trials from different conditions using independent-samples t tests and then applied a two-tailed threshold of $p = 0.05$ to the t values. Adjacent time points exceeding the threshold were grouped together into clusters for which the sum of t values was calculated. These procedures were repeated using the Monte Carlo method with 10,000 permuted randomizations of trials (using all insular cortex electrodes within a given subject for iEEG data and thus correcting for multiple comparisons). Observed clusters with a corrected, two-tailed Monte Carlo significance probability of <0.05 were considered as significant. We then focused our main subsequent analyses on the maximally responsive insular cortex electrode within each subject that showed clusters of significantly increased HFB for (1) correct omissions compared with correct commissions, (2) commission errors compared with correct commissions, and (3) commission errors compared with correct omissions.

For the maximally responsive insula electrodes, we compared the magnitude and timing of the HFB signal with normalized pupil response on a trial-by-trial basis for target trials (both correct omissions and commission errors). For each of these trials, we performed cross-correlation between the insula and pupil time series using shifts of -3 to 3 s. We also computed the Pearson correlation coefficient between peak HFB values in the insula (within the 0 to 2 s post-trial onset window) and peak normalized pupil diameter values (within the 0 to 3 s post-trial onset window).

Receiver operating characteristic (ROC) curve analysis. We used ROC curves to define amplitude and duration thresholds that optimally captured “activations” within continuous time series. For each subject, the main analysis was performed for the maximally responsive insula electrode (as defined based on cluster-based permutation testing). In line with previous work (Dastjerdi et al., 2013), we smoothed the HFB signal with a 500 ms Gaussian kernel to capture local trends. To identify parameters that optimally discriminated task-evoked responses from baseline activity on a trial-by-trial basis, we split trials into target (all mountains, except for those that were preceded by mountains) and baseline (a random subsample of correct commission trials, matching the total number of mountain trials within each run). For each trial, within the window of 0 – 2 s post-trial onset, we evaluated whether an “activation” was present when applying a range of combined amplitude (0.5 – 3 in increments of 0.5) and duration (0.25 – 1 in increments of 0.25) thresholds to the HFB signal. For the ROC curves, we defined four classes of trials: (1) true positive (activation for target trial); (2) false negative (no activation for target trial); (3) true negative (no activation for baseline trial); and (4) false positive (activation for baseline trial). We defined the optimal combination of amplitude and duration thresholds based on the ROC curve data point that minimized both false negatives and false positives (i.e., was closest to the top left).

In the continuous HFB signals of task and rest runs, we defined daIC activations as all instances in which the optimal ROC curve-based duration and amplitude thresholds were both surpassed. We quantified these discrete events in terms of activations per minute across all runs within each condition (ignoring remainder segments and the ends of runs that were <1 min). We compared the daIC activations per minute in task compared with rest recordings within subject (Wilcoxon rank sum test, significance set at $p < 0.05$). We also compared HFB power amplitude (based on the unsmoothed time course) between task and rest, using the -50 to 50 ms window surrounding HFB peaks for all instances of HFB

activations in each condition (Wilcoxon rank sum test, significance set at $p < 0.05$). Additionally, given that activations tended to cluster together closely in time but otherwise showed variable interactivation intervals that might differ between conditions, we fit the distribution of interactivation intervals with an ex-Gaussian function that assumed a mixture of Gaussian and exponential distributions (Lacouture and Cousineau, 2008). We fit the parameters μ (mean of Gaussian component) and τ (mean of the exponential component) to the interactivation interval data separately for task and rest sessions.

Pupil responses aligned to iEEG events. Surrounding the daIC peak HFB signal value for each daIC activation event, we defined an epoch in the pupil time series (-0.8 to 3 s relative to the daIC peak) and subtracted out the pre-daIC peak (-0.8 to 0 s) mean pupil size values (see Pupil data preprocessing). We averaged the pupil time series across all daIC-aligned trials (merged across runs), separately for task and rest. For task analyses, we additionally computed these averages separately for daIC peaks that followed target trials (defined as being within the first 2 s following the onset of mountain stimuli) versus those that did not directly follow target onsets.

To assess the statistical significance of pupil responses to daIC activations, we generated null pupil responses from the same dataset. Within each run, we computed the interevent intervals between all daIC activations. We then randomly shuffled these interevent interval values such that the event-timing distribution was preserved, but individual events were no longer aligned to daIC activations. We then extracted pupil time series within epochs (-0.8 to 3 s) surrounding shuffled onsets. We implemented the same pupil processing and trial exclusion criteria as applied to the daIC-aligned epochs. We averaged the pupil time series across all null trials (merged across runs) to obtain a null pupil response. We then repeated these procedures with 10,000 iterations to obtain a distribution of null pupil responses. For each iteration, we computed the area under the curve (AUC), defined as the mean null trial response minus 1 SE in the 0 to 3 s window relative to daIC event onset. This resulted in a null AUC distribution that we used to obtain a p value for the daIC-aligned pupil AUC. For analyses of all insular cortex electrodes that showed significant task-evoked HFB responses, we applied false discovery rate correction to these p values within subjects.

Results

Functional localization of daIC

We recorded from 62 unique sites within human insular cortex across 3 subjects (Fig. 1*a*). In each subject, the epileptic foci were found to be outside the insular cortex (Table 1). No ictal or interictal was recorded in the daIC throughout clinical monitoring over the course of 5–10 d. Subjects performed between 4 and 8 runs (6 min each) of the GradCPT (Esterman et al., 2013) (Fig. 1*b*) with simultaneous pupillometry. In the task condition, subjects viewed a continuously changing visual stream of luminance-matched images and were instructed to press a button each time they saw a city (frequent category, $\sim 90\%$ of all stimuli) and to withhold their response when they saw a mountain (infrequent category, $\sim 10\%$ of all stimuli) (for summaries of behavioral performance, see Table 1).

To capture electrophysiological activations, we focused on HFB (70–170 Hz) activity, an index of neuronal population activity (Parvizi and Kastner, 2018). We screened electrodes within the insula for selective HFB responses to target stimuli (mountains) during trials with correct (withheld button press) and incorrect (button press) behavioral responses. Across the 3 subjects, we identified 21 insula electrodes that showed significant HFB responses during target (mountain) compared with nontarget (city) trials (Monte Carlo $p < 0.05$, cluster-based permutation test, corrected for all insula electrodes within subject). Among active electrodes, 9 (at least 1 per subject) showed an additional

effect of significantly greater HFB response for trials with incorrect relative correct behavioral responses (Monte Carlo $p < 0.05$, cluster-based permutation test, corrected for all insula electrodes within subject), consistent with an “error monitoring” response that has been reported previously in the daIC and salience network (Dosenbach et al., 2006; Bastin et al., 2017; Fortenbaugh et al., 2018; Kucyi et al., 2020). This response profile has been previously reported in fMRI for both errors of commission and omission (Fortenbaugh et al., 2018); and we also confirmed that, when task instructions were reversed (i.e., press for infrequent category, no press for frequent category), similar daIC HFB responses were found during infrequent target trials (unpublished data).

The responsive electrodes in the 3 subjects were largely clustered within the daIC, and electrodes showing an error-monitoring response profile were found exclusively within the daIC (Fig. 1*c*). We focused our subsequent main analyses on the daIC neuronal population within each subject that showed the strongest task-evoked HFB increase (shown on sagittal slices in Fig. 1*c*). The peak-responsive daIC site for each subject was within the salience network, as defined based on a normative atlas of intrinsic networks (Fig. 1*d*) (for MNI coordinates, see Table 1).

Task-evoked daIC activation scales with subsequent pupil dilation

We next tested the hypothesis that task-evoked daIC activation is temporally coupled with pupil dilation. In each subject, the daIC showed a sharp HFB increase following the onset of target stimuli (peaking at ~ 0.8 to 1 s after the stimulus began fading in) (Fig. 2*a*). For behavioral error compared with correct trials, temporal clusters of significantly increased HFB amplitude were found during the later phase of the response (Fig. 2*b*, top, red lines). Additionally, in each subject, the pupil size significantly increased following the onset of target compared with nontarget trials (Monte Carlo $p < 0.05$, cluster-based permutation test) (Fig. 2*c*). The pupil showed a relatively slow and sustained response, peaking 1–3 s after target fade-in onset, consistent with the expected task-evoked pupil dilation profile widely seen during cognitive effort and arousal in healthy adults (Mathôt, 2018). For error compared with correct trials, pupil dilations were of similar magnitude in 2 subjects (S1 and S2) but were significantly stronger in one subject (S3; i.e., mirroring the daIC response).

Trial-by-trial cross-correlations highlighted that pupil dilations consistently lagged behind task-evoked daIC HFB activations (Fig. 2*c*). The pupil reached its maximum size with a variable mean delay among subjects following daIC activation peaks (S1, 564 ms; S2, 508 ms; S3, 1200 ms). Critically, the magnitude of daIC HFB activation on a trial-by-trial basis was correlated with the degree of pupil size increase within each subject (S1: $r = 0.16$, $p = 0.06$; S2: $r = 0.19$, $p = 0.005$; S3: $r = 0.36$, $p = 0.0002$) (Fig. 2*d*). These findings suggest either that task-evoked daIC activation could causally drive pupil dilation or that a common source can elicit both daIC activation and pupil dilation.

Spontaneous daIC activations are detected during wakeful rest

Having established a reliable relationship between task-evoked daIC neuronal population activity and pupillary responses within each subject, we next aimed to “tag” individual instances of daIC activation during a wakeful state of spontaneous cognition, also known as the “resting state” (in a manner similar to that applied in countless neuroimaging studies of resting-state functional

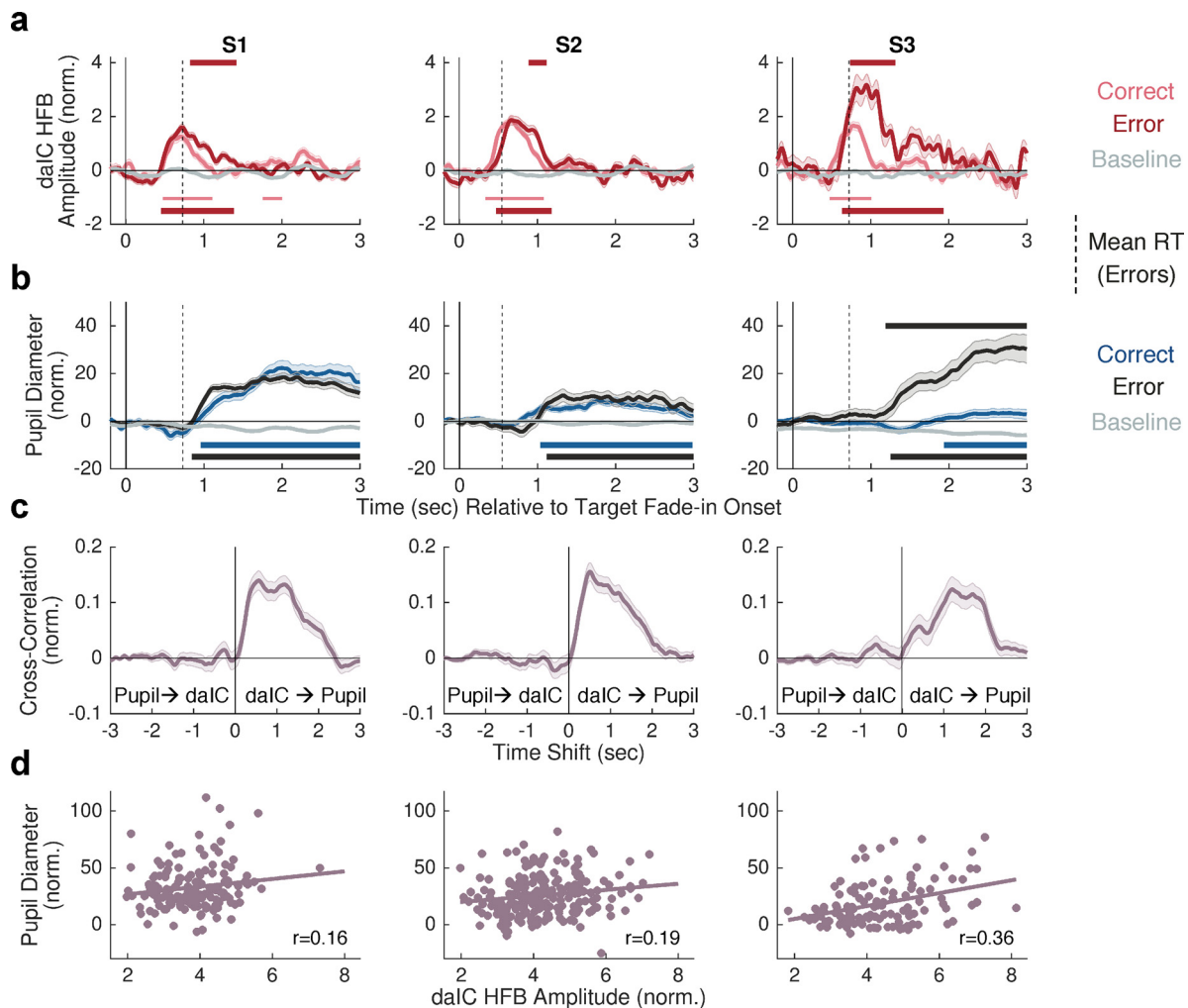


Figure 2. Temporal coupling between task-evoked daIC activation and pupil dilation. **a**, Mean HFB power amplitude at peak-responsive daIC electrodes for target trials with correct behavioral responses (pink), target trials with erroneous behavioral responses (red), and nontarget trials with correct behavioral response (gray, considered as baseline). **b**, Mean changes in pupil diameter for correct (blue), incorrect (black), and baseline (gray) trials. **a**, **b**, Dashed vertical lines indicate the mean reaction time for target trials with erroneous behavioral responses. **c**, Cross-correlation (averaged across all target trials) between daIC HFB amplitude and pupil diameter. **d**, Trial-by-trial correlation (for all target trials) between daIC HFB amplitude and pupil diameter change. In all relevant plots, shaded error bars indicate SEM.

connectivity). Although “spontaneous cognition state” is a more accurate depiction of this state where the participants’ cognitive processing did not rely on a known event structure in the external environment, we use the term “rest” or “resting state” to relate to past neuroimaging studies.

To define daIC activation events at rest, we first used ROC curves to obtain parameters that optimally describe the amplitude and duration of task-evoked HFB activation (Dastjerdi et al., 2013). To characterize daIC activations, for each target trial in the GradCPT, we defined activation as a “true-positive” and no activation as a “false-negative” observation (Fig. 3*a*). For nontarget trials, we defined activation as “false-positive” and no activation as “true-negative.” Using multiple combined pairs of candidate HFB amplitude and duration thresholds for a given electrode, we obtained ROC curves and identified the amplitude-duration pair that resulted in optimal sensitivity and specificity (e.g., Fig. 3*b*, data point with black outline). For the daIC electrodes in the 3 subjects, this procedure resulted in peak sensitivity/specificity values of 0.68/0.70 (S1), 0.68/0.83 (S2), and 0.71/0.79 (S3). This trial-type discrimination was not as strong as that reported previously in parietal cortex for a distinct, controlled

cognitive task that included explicit rest periods as baseline (Dastjerdi et al., 2013). However, given that the continuous performance task used here involves rapid trial transitions, requires a higher “baseline” level of attention, and is associated with frequent fluctuations of attention (Esterman et al., 2013; Kucyi et al., 2016), an increased level of unsystematic HFB activity dynamics was expected.

Using the optimal HFB amplitude/duration thresholds obtained from ROC curves, we tagged all daIC activations that occurred during the GradCPT as well as during the resting-state condition. Activations were found to emerge regularly during rest (Fig. 3*c*). During both task and rest, activations tended to occur in closely spaced “bursts” (within ~1–3 s of one another) interspersed with intervals of varying durations on the order of tens of seconds, with a longer exponential tail on the distribution of interactivation intervals in rest compared with task (Fig. 3*d*). The rate of daIC activations per minute was significantly reduced during rest, compared with task, within each subject (S1: $p = 0.025$; S2: $p = 0.0011$; S3: $p = 0.039$; Wilcoxon rank-sum tests) (Fig. 3*e*). Thus, although our findings confirm that daIC activations intermittently emerged spontaneously, the frequency of

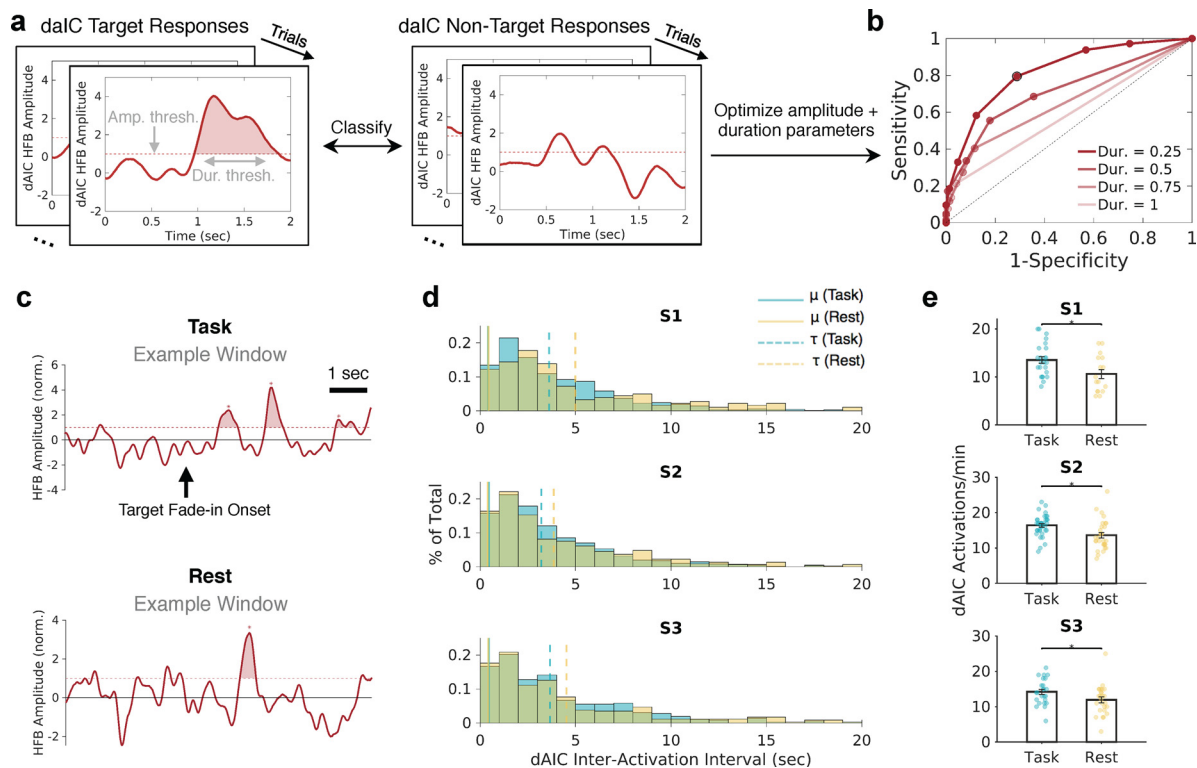


Figure 3. daIC activations are detected during wakeful rest but are reduced in frequency. *a*, Example of the presence and absence of daIC activation during GradCPT target and nontarget trials, given selected amplitude and duration thresholds. *b*, Example ROC curve for a single daIC electrode based on multiple pairs of candidate amplitude and duration thresholds. The pair that resulted in optimized sensitivity and specificity for trial discrimination is outlined in black. *c*, Example 8 s segments showing daIC activations derived from ROC curves during task and rest conditions. Shaded areas represent suprathreshold events. *d*, Histograms represent daIC interactivation intervals across all task and rest sessions within each subject. Based on ex-Gaussian fits, the Gaussian mean (μ , solid vertical lines) and exponential mean (τ , dotted vertical lines) are shown for task and rest. *e*, Activation rates in the daIC, across independent 1 min windows, for task compared with rest within each subject. * $p < 0.05$ (Wilcoxon rank-sum test).

these activations was consistently reduced compared with during GradCPT performance.

Spectral similarity between task-evoked and spontaneous daIC activation

We next aimed to further characterize the potential similarity between rest and task-evoked activations. We therefore investigated electrophysiological spectral properties beyond the HFB frequency range used to define the activations. Spectrograms showing power amplitude for frequencies ranging from 1 to 170 Hz revealed striking signal similarities between task-evoked and resting-state HFB activation events (Fig. 4*a*). In both conditions, transient HFB activations were coupled to decreased power amplitude in lower-frequency bands, consistent with the typical iEEG spectral profile seen during increased neuronal population activity (Miller et al., 2007).

To compare spectral properties during HFB activations between task and rest conditions, we computed power amplitudes within lower-frequency ranges from 4 to 70 Hz (i.e., outside the HFB range used to define the activations). This revealed similar spectral profiles between HFB activations during task and rest, with increased power amplitude found selectively within the higher frequency range (70–170 Hz, sometimes extending to 40–70 Hz) (Fig. 4*b*). However, the mean HFB amplitude was stronger for task and compared with rest activations ($p < 0.01$ with each subject, Wilcoxon rank-sum tests). Thus, although spontaneous activations were on average of lower magnitude than task-

evoked activations, spectrotemporal properties were largely preserved across conditions.

Spontaneous insula activation precedes pupil dilation

Having established that resting-state and task-evoked activations had shared electrophysiological properties, we next tested the hypothesis that spontaneous activations are time-locked to pupil dilation. We aligned the pupil size time course to each daIC activation peak (Fig. 5*a*) and then computed the mean of daIC-aligned pupil size during task and rest. For a null comparison, we aligned the pupil to 10,000 permutations of randomly shuffled distributions of daIC interactivation intervals.

As anticipated from our prior analysis of task-evoked responses (Fig. 2), we first confirmed that pupil size showed a strong and sustained increase following daIC activations during task performance (Fig. 5*b*). The AUC for daIC-aligned pupil responses during task performance was significantly greater than that for the null distribution ($p < 0.001$ for each subject). Although this daIC-aligned pupil response was particularly strong for daIC activations that followed target trials, also noted was an increase in pupil size (of smaller relative magnitude) following daIC activations that were during nontarget trials rather than immediately after target trials (Fig. 6). This suggests that daIC-aligned pupil dilations occurred not only while processing behaviorally relevant target stimuli but also on instances of daIC activations during habitual behavioral responses to nontarget stimuli.

Our key analysis, however, was focused on whether pupil dilations followed task-like daIC activations during a resting state in the absence of externally triggered cognitive changes. Critically, during rest (i.e., continuous visual fixation on an unchanging stimulus), the pupil showed daIC-aligned responses with a time course that was strikingly similar to that found during task performance in each subject (Fig. 5c). The AUC of these pupil responses during wakeful rest was significantly greater than that for the null distribution (S1: $p = 0.0065$, S2: $p = 0.050$; S3: $p = 0.0037$). The delay of the pupillary response relative to daIC activation was comparable across conditions within subjects, as estimated based on the mean daIC-pupil cross-correlation derived from all instances of daIC activation (S1: task = 520 ms, rest = 492 ms; S2: task = 524 ms, rest = 712 ms, S3: task = 1240 ms, rest = 1740 ms).

We expanded this analysis to all task-responsive insular cortex electrodes within subjects and found that HFB activations at rest were associated with significant subsequent pupil dilation for 16 total recording sites that were largely within the left and right daIC ($p_{\text{FDR}} < 0.05$) (Fig. 5d). Indeed, within each subject, the majority (76%) of electrodes that showed significant task-evoked activation also showed a significant relationship between spontaneous activation and pupil dilation (S1, 2 of 3 electrodes; S2, 7 of 10 electrodes; S3, 7 of 8 electrodes). These findings confirm that the daIC activations are temporally coupled to pupil dilations, regardless of whether the daIC activations are task-evoked or spontaneous.

Discussion

In summary, we have reported several novel findings: (1) spontaneous daIC activations occur within the same neuronal populations and with the same spectrotemporal profiles as task-evoked activations; (2) spontaneous daIC activations are time locked to pupillary responses in a manner similar to task-evoked brain and pupillary responses; and (3) task-evoked responses directly recorded from human daIC, sensitive to behavioral errors, precede and correlate with the magnitude of evoked pupil dilations. Building on prior functional neuroimaging studies (X. Liu and Duyn, 2013; Karahanoğlu and Van De Ville, 2015), our findings provide support from direct human intracranial recordings for similar neurophysiological profiles between spontaneous and task-evoked activations and additionally highlight a novel link between these activations and autonomic functions measured by dynamics of pupillary dilation.

Sympathetic pathways within the autonomic nervous system play a key role in the neural control of pupil size, and our findings must be considered within the context of these well-described systems. Pupil dilation is mediated by sympathetic activity originating in the hypothalamus and that signals to the intermediolateral column of the spinal cord and superior cervical ganglion to engage the iris dilator muscle (Wang and Munoz, 2015; Y. Liu et al., 2017; Mathôt, 2018). Electrical stimulation of

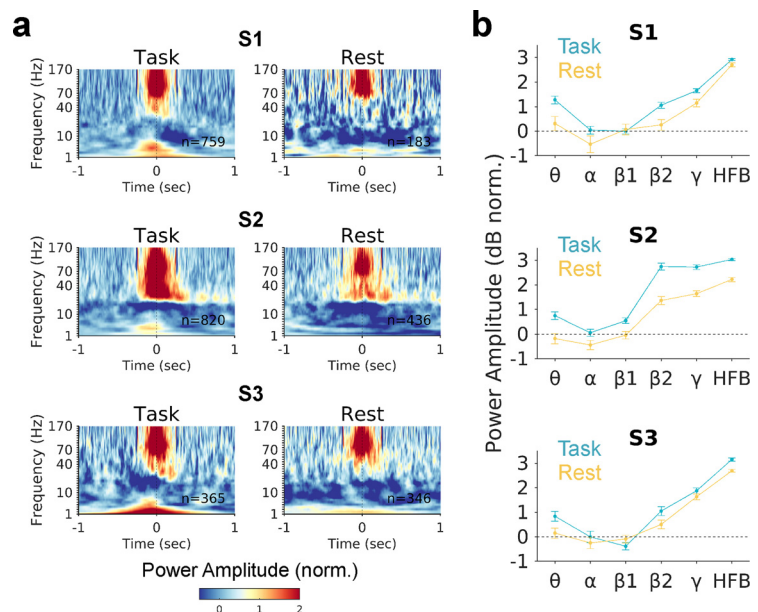


Figure 4. Similar electrophysiological spectral properties between task-evoked and spontaneous daIC activation. **a**, Mean spectrograms, in task and wakeful resting state, aligned to HFB peaks ($t = 0$) defined based on ROC curves in task and rest. **b**, Mean power amplitude in the -50 to 50 ms window surrounding HFB peaks for the θ (4–8 Hz), α (8–12 Hz), β_1 (13–29 Hz), β_2 (30–39 Hz), γ (40–70 Hz), and HFB ranges.

the locus ceruleus and superior colliculus results in pupil dilation (Wang et al., 2014; Joshi et al., 2016; Reimer et al., 2016), suggesting a direct interaction with the circuitry for pupil control, although anatomic connections that could mediate these interactions are not fully known. It has often been assumed that the covariation between pupil size and electrophysiological activity in cortical areas, such as the dorsal anterior-/mid-cingulate cortex, reflects interactions with the locus ceruleus-noradrenaline system (Ebitz and Platt, 2015; Joshi et al., 2016).

We are unaware of previous research linking insular cortex electrophysiological dynamics with pupil size. Our highly consistent findings within single subjects are concordant with previous fMRI studies that relied on group-level inferences and slower hemodynamic activity (Murphy et al., 2014; Schneider et al., 2016; Breeden et al., 2017). Multiple lines of evidence suggest that the daIC is tightly integrated with the autonomic nervous system (Uddin, 2015), yet the structural and functional connectivity patterns that could support interactions with pupil control circuitry are not fully understood. The daIC is among multiple cortical and subcortical regions that have been implicated in a “central autonomic network,” including the anterior mid-cingulate cortex, amygdala, ventromedial PFC, inferior and medial frontal gyrus, and posterior insula (Benarroch, 1993; Beissner et al., 2013; Cechetto, 2014; Ruiz Vargas et al., 2016). The daIC projects to the anterior mid-cingulate cortex within the nonhuman primate (Mesulam and Mufson, 1982; Vogt and Pandya, 1987), a region that has also been consistently implicated in pupil dilation during cognitive and autonomic processing (Critchley et al., 2005; Ebitz and Platt, 2015). In humans, these regions show intrinsic functional connectivity with one another as well as more broadly with the salience network, including cortical and subcortical sites that may support autonomic control (Seeley et al., 2007; Taylor et al., 2009). The salience network activity is sensitive to neuromodulatory activity within the noradrenergic system (Hermans et al., 2011), potentially supporting

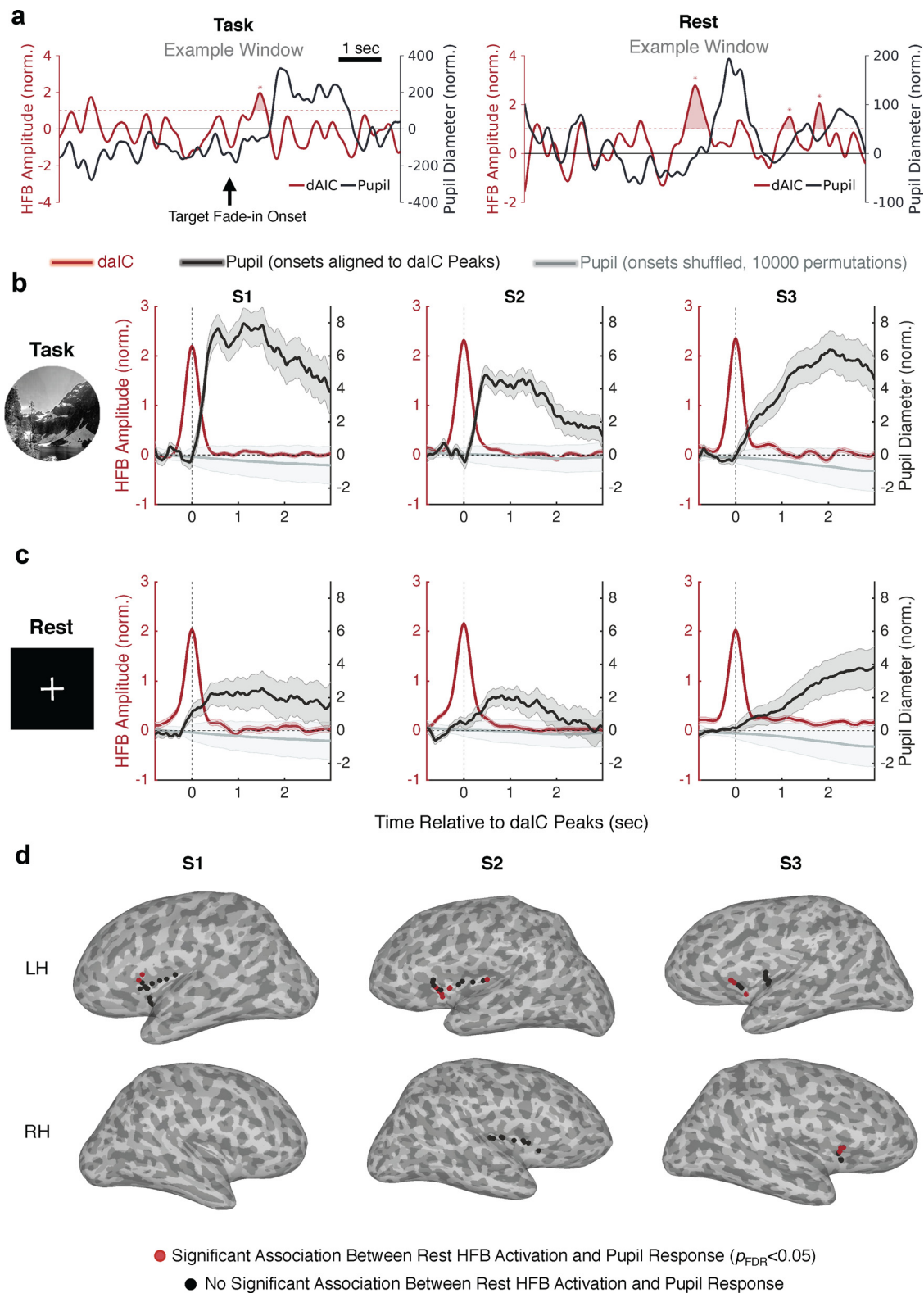


Figure 5. daIC activations precede evoked and spontaneous pupil dilations. **a**, Example 8 s segments showing ROC-derived daIC activations and pupil size fluctuations during task and rest conditions (examples were selected for illustrative purposes only and were not necessarily representative of mean effects). **b**, Pupil response (black) aligned to daIC HFB activation (red) peaks in each subject during task performance. **c**, Same as in **a**, but during wakeful rest (continuous visual fixation). Gray lines indicate the mean pupil response for 10,000 randomly shuffled distributions of daIC interactivation intervals. **d**, Insular cortex electrodes within each subject that either showed a significant association between HFB activation and subsequent increased pupil size (red) or did not show a significant association (black) during wakeful rest. Shaded error bars indicate SEM.

the idea that the daIC may be integrated with pupil control circuitry via interactions with the locus ceruleus. It should be acknowledged, however, that pupil size dynamics likely reflect a complex interplay of multiple neuromodulatory systems and are not necessarily a pure index of locus ceruleus or noradrenergic activity (McGinley et al., 2015; Reimer et al., 2016; Joshi and Gold, 2020).

Beyond pupil size, spontaneous anterior insula activity and functional connectivity have been linked to various other autonomic system measures, such as heart rate and skin conductance, in fMRI studies (Fan et al., 2012; Chang et al., 2013; James et al., 2013; Valenza et al., 2019). Intrinsic fMRI connectivity of the anterior insula is also associated with individual differences in autonomic physiological function within neurologic patients (Guo et al., 2016; Taylor et al., 2016). Moreover, intracranial electrical stimulation of the insular cortex, including the daIC, results in various profiles of cardiac response, suggesting causal roles in both sympathetic and parasympathetic functions (Oppenheimer et al., 1992; Chouchou et al., 2019). Future work is needed to determine whether the daIC similarly has a causal role in pupil control.

Beyond being implicated in autonomic functions, a highly replicated finding in prior fMRI and iEEG studies is that the daIC is activated during the inhibition of motor activity (i.e., “stopping”) and during failure to inhibit motor activity (Dosenbach et al., 2006; Cai et al., 2014; Bastin et al., 2017), as confirmed here. This stop, or “braking,” signal (Aron et al., 2014) is typically also found in an adjacent region in the inferior frontal gyrus, although the daIC and inferior frontal gyrus response profiles are partially dissociable (Cai et al., 2014). It has been suggested that this signal could underlie the stopping of internal goals (Aron et al., 2014), which offers one potential account of the spontaneous activations detected here. However, it remains to be determined whether the daIC activations during “no-go” trials may be related to the heightened salience of these trials (similar to infrequent mountain trials in our task) rather than the inhibition of motor responses per se.

Our findings build on a growing body of evidence suggesting that specific components of spontaneous brain activity, embedded within an intrinsic functional architecture, have relevance to immediate cognitive and physiological processes (Kucyi et al., 2018a). What types of cognitive processes might spontaneous daIC-pupil coupling reflect? It has been suggested that spontaneous neural activation exceeding a dynamic threshold can be described as a “nonlinear ignition” that leads to awareness of either external or internal phenomena (Moutard et al., 2015). Within this context, it has been suggested that neural activations before pupil dilation may signify awareness of spontaneous thought (Moutard et al., 2015; Yellin et al., 2015). However, it is unlikely that pupil dilation shows a one-to-one relationship with self-generated experiences (Smallwood et al., 2011; Mittner et al., 2014; Unsworth and Robison, 2016; Konishi et al., 2017). Given the role of the daIC in alerting, salience detection, and error monitoring (Menon and Uddin, 2010; Uddin, 2015), it is possible that spontaneous activation reflects intermittent monitoring of the external and internal environments for behaviorally relevant information. An additional possibility is that spontaneous

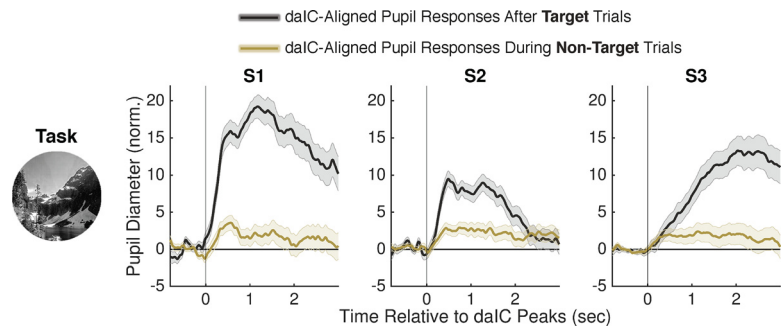


Figure 6. daIC activations precede pupil dilations during both target and nontarget trials in the GradCPT. Pupil response aligned to daIC HFB activation peaks ($t = 0$), split based on daIC peaks that were found after target trials (black) and during nontarget trials (olive) while patients were performing the GradCPT.

daIC activations arise from interoceptive signals, including prediction errors (analogous to the externally generated daIC error-monitoring signals observed during task performance) (Barrett and Simmons, 2015; Livneh et al., 2020). Future confirmatory studies ought to involve subjective reports and/or behavioral measures following instances of spontaneous neural activation coupled to pupil dilation.

A related limitation of our work is that we were unable to report on activations from brain regions other than the insula, given the heterogeneous coverage of electrodes across subjects within our sample. Recordings from primary sensory or motor areas may have given insight into whether, during the resting-state condition, subjects were engaged in self-generated thoughts versus attention to exteroceptive input. For example, in human primary auditory cortex, stimulus-evoked activations (i.e., increases in spiking rate) are distinguishable from low-amplitude fluctuations found in spontaneous activity (Nir et al., 2008). Additionally, recordings of spontaneous activity from higher-order brain areas, such as default mode network regions that are implicated in self-generated cognitive processes and that exhibit transient, high-amplitude electrophysiological activations during the resting state (similar to those found in the insula here) (Dastjerdi et al., 2011; Daitch and Parvizi, 2018), could provide further clues about the cognitive relevance of dynamic interactions between spontaneous pupillary and neural fluctuations.

Although our study was focused on within-individual relationships between the insula and pupil (and all effects were replicated within each subject), there were notable individual differences in the timing of the daIC-pupil relationship. Subject S3, in particular, exhibited an increased latency of the pupil relative to the daIC in both task and rest conditions (see Figs. 2c, 5b,c). This subject was older than the other patients (Table 1), and it has been shown that pupillary dilation latency increases as a function of age (Bitsios et al., 1996). This subject’s mean reaction was also slower than that of the other patients (Table 1), potentially suggesting that the delayed pupil timing could be related to processing speed. However, a future study of a larger cohort would be needed to formally investigate such hypotheses concerning the source of individual differences.

In conclusion, our work provides unique and novel evidence for a link between brief, spontaneous activations within human insular cortex and pupil dilation. We suggest that this association arises from coordination of the insula with a distributed network of cortical and subcortical areas that are tightly integrated with autonomic and neuromodulatory systems. Our approach of

tagging task-like, spontaneous neural activations could be extended and combined with various behavioral and physiological measures to further delineate the functional significance of intrinsic activity within broader brain networks.

References

- Aron AR, Robbins TW, Poldrack RA (2014) Inhibition and the right inferior frontal cortex: one decade on. *Trends Cogn Sci* 18:177–185.
- Aston-Jones G, Cohen JD (2005) An integrative theory of locus ceruleus-norepinephrine function: adaptive gain and optimal performance. *Annu Rev Neurosci* 28:403–450.
- Barrett LF, Simmons WK (2015) Interoceptive predictions in the brain. *Nat Rev Neurosci* 16:419–429.
- Bastin J, Deman P, David O, Gueguen M, Benis D, Minotti L, Hoffman D, Combrisson E, Kujala J, Perrone-Bertolotti M, Kahane P, Lachaux JP, Jerbi K (2017) Direct recordings from human anterior insula reveal its leading role within the error-monitoring network. *Cereb Cortex* 27:1545–1557.
- Beissner F, Meissner K, Bar KJ, Napadow V (2013) The autonomic brain: an activation likelihood estimation meta-analysis for central processing of autonomic function. *J Neurosci* 33:10503–10511.
- Benarroch EE (1993) The central autonomic network: functional organization, dysfunction, and perspective. *Mayo Clin Proc* 68:988–1001.
- Bitsios P, Prettyman R, Szabadi E (1996) Changes in autonomic function with age: a study of pupillary kinetics in healthy young and old people. *Age Ageing* 25:432–438.
- Brainard DH (1997) The Psychophysics Toolbox. *Spat Vis* 10:433–436.
- Breeden AL, Siegle GJ, Norr ME, Gordon EM, Vaidya CJ (2017) Coupling between spontaneous pupillary fluctuations and brain activity relates to inattentiveness. *Eur J Neurosci* 45:260–266.
- Cai W, Ryali S, Chen T, Li CS, Menon V (2014) Dissociable roles of right inferior frontal cortex and anterior insula in inhibitory control: evidence from intrinsic and task-related functional parcellation, connectivity, and response profile analyses across multiple datasets. *J Neurosci* 34:14652–14667.
- Cechetti DF (2014) Cortical control of the autonomic nervous system. *Exp Physiol* 99:326–331.
- Chang C, Metzger CD, Glover GH, Duyn JH, Heinze HJ, Walter M (2013) Association between heart rate variability and fluctuations in resting-state functional connectivity. *Neuroimage* 68:93–104.
- Chouchou F, Mauguier F, Vallayer O, Catenox H, Isnard J, Montavont A, Jung J, Pichot V, Rheims S, Mazzola L (2019) How the insula speaks to the heart: cardiac responses to insular stimulation in humans. *Hum Brain Mapp* 40:2611–2622.
- Craig AD (2009) How do you feel–now? The anterior insula and human awareness. *Nat Rev Neurosci* 10:59–70.
- Critchley HD, Tang J, Glaser D, Butterworth B, Dolan RJ (2005) Anterior cingulate activity during error and autonomic response. *Neuroimage* 27:885–895.
- Daitch AL, Parvizi J (2018) Spatial and temporal heterogeneity of neural responses in human posteromedial cortex. *Proc Natl Acad Sci USA* 115:4785–4790.
- Dastjerdi M, Foster BL, Nasrullah S, Rauschecker AM, Dougherty RF, Townsend JD, Chang C, Greicius MD, Menon V, Kennedy DP, Parvizi J (2011) Differential electrophysiological response during rest, self-referential, and non-self-referential tasks in human posteromedial cortex. *Proc Natl Acad Sci USA* 108:3023–3028.
- Dastjerdi M, Ozker M, Foster BL, Rangarajan V, Parvizi J (2013) Numerical processing in the human parietal cortex during experimental and natural conditions. *Nat Commun* 4:2528.
- Dosenbach NU, Visscher KM, Palmer ED, Miezin FM, Wenger KK, Kang HC, Burgund ED, Grimes AL, Schlaggar BL, Petersen SE (2006) A core system for the implementation of task sets. *Neuron* 50:799–812.
- Downar J, Crawley AP, Mikulis DJ, Davis KD (2002) A cortical network sensitive to stimulus salience in a neutral behavioral context across multiple sensory modalities. *J Neurophysiol* 87:615–620.
- Ebitz RB, Platt ML (2015) Neuronal activity in primate dorsal anterior cingulate cortex signals task conflict and predicts adjustments in pupil-linked arousal. *Neuron* 85:628–640.
- Esterman M, Noonan SK, Rosenberg M, Degutis J (2013) In the zone or zoning out? Tracking behavioral and neural fluctuations during sustained attention. *Cereb Cortex* 23:2712–2723.
- Fan J, Xu P, Van Dam NT, Eilam-Stock T, Gu X, Luo YJ, Hof PR (2012) Spontaneous brain activity relates to autonomic arousal. *J Neurosci* 32:11176–11186.
- Fischl B, Sereno MI, Tootell RB, Dale AM (1999) High-resolution intersubject averaging and a coordinate system for the cortical surface. *Hum Brain Mapp* 8:272–284.
- Fortenbaugh FC, Rothlein D, McGlinchey R, DeGutis J, Esterman M (2018) Tracking behavioral and neural fluctuations during sustained attention: a robust replication and extension. *Neuroimage* 171:148–164.
- Foster BL, Rangarajan V, Shirer WR, Parvizi J (2015) Intrinsic and task-dependent coupling of neuronal population activity in human parietal cortex. *Neuron* 86:578–590.
- Fox MD, Raichle ME (2007) Spontaneous fluctuations in brain activity observed with functional magnetic resonance imaging. *Nat Rev Neurosci* 8:700–711.
- Groppe DM, Bickel S, Dykstra AR, Wang X, Megevand P, Mercier MR, Lado FA, Mehta AD, Honey CJ (2017) iELVis: an open source MATLAB toolbox for localizing and visualizing human intracranial electrode data. *J Neurosci Methods* 281:40–48.
- Guo CC, Sturm VE, Zhou J, Gennatas ED, Trujillo AJ, Hua AY, Crawford R, Stables L, Kramer JH, Rankin K, Levenson RW, Rosen HJ, Miller BL, Seeley WW (2016) Dominant hemisphere lateralization of cortical parasympathetic control as revealed by frontotemporal dementia. *Proc Natl Acad Sci USA* 113:2430–2439.
- Hermans EJ, van Marle HJ, Ossewaarde L, Henckens MJ, Qin S, van Kesteren MT, Schoots VC, Cousijn H, Rijpkema M, Oostenveld R, Fernández G (2011) Stress-related noradrenergic activity prompts large-scale neural network reconfiguration. *Science* 334:1151–1153.
- James C, Henderson L, Macefield VG (2013) Real-time imaging of brain areas involved in the generation of spontaneous skin sympathetic nerve activity at rest. *Neuroimage* 74:188–194.
- Joshi S, Gold JJ (2020) Pupil size as a window on neural substrates of cognition. *Trends Cogn Sci* 24:466–480.
- Joshi S, Li Y, Kalwani RM, Gold JJ (2016) Relationships between pupil diameter and neuronal activity in the locus ceruleus, colliculi, and cingulate cortex. *Neuron* 89:221–234.
- Karahanoglu FI, Van De Ville D (2015) Transient brain activity disentangles fMRI resting-state dynamics in terms of spatially and temporally overlapping networks. *Nat Commun* 6:7751.
- Kiebel SJ, Friston KJ (2004) Statistical parametric mapping for event-related potentials: I. Generic considerations. *Neuroimage* 22:492–502.
- Konishi M, Brown K, Battaglini L, Smallwood J (2017) When attention wanders: pupillometric signatures of fluctuations in external attention. *Cognition* 168:16–26.
- Kucyi A, Esterman M, Riley CS, Valera EM (2016) Spontaneous default network activity reflects behavioral variability independent of mind-wandering. *Proc Natl Acad Sci USA* 113:13899–13904.
- Kucyi A, Tambini A, Sadaghiani S, Keilholz S, Cohen JR (2018a) Spontaneous cognitive processes and the behavioral validation of time-varying brain connectivity. *Netw Neurosci* 2:397–417.
- Kucyi A, Schrouff J, Bickel S, Foster BL, Shine JM, Parvizi J (2018b) Intracranial electrophysiology reveals reproducible intrinsic functional connectivity within human brain networks. *J Neurosci* 38:4230–4242.
- Kucyi A, Daitch A, Raccach O, Zhao B, Zhang C, Esterman M, Zeineh M, Halpern CH, Zhang K, Zhang J, Parvizi J (2020) Electrophysiological dynamics of antagonistic brain networks reflect attentional fluctuations. *Nat Commun* 11:325.
- Lacouture Y, Cousineau D (2008) How to use MATLAB to fit the ex-Gaussian and other probability functions to a distribution of response times. *Tutor Quant Methods Psychol* 4:35–45.
- Li X, Liang Z, Kleiner M, Lu ZL (2010) RTbox: a device for highly accurate response time measurements. *Behav Res Methods* 42:212–225.
- Liu X, Duyn JH (2013) Time-varying functional network information extracted from brief instances of spontaneous brain activity. *Proc Natl Acad Sci USA* 110:4392–4397.
- Liu Y, Rodenkirch C, Moskowitz N, Schriver B, Wang Q (2017) Dynamic lateralization of pupil dilation evoked by locus ceruleus activation results from sympathetic, not parasympathetic, contributions. *Cell Rep* 20:3099–3112.

- Livneh Y, Sugden AU, Madara JC, Essner RA, Flores VI, Sugden LA, Resch JM, Lowell BB, Andermann ML (2020) Estimation of current and future physiological states in insular cortex. *Neuron* 105:1094–1111.e110.
- Maris E, Oostenveld R (2007) Nonparametric statistical testing of EEG- and MEG-data. *J Neurosci Methods* 164:177–190.
- Mathôt S (2018) Pupillometry: psychology, physiology, and function. *J Cogn* 1:16.
- McGinley MJ, Vinck M, Reimer J, Batista-Brito R, Zagha E, Cadwell CR, Tolias AS, Cardin JA, McCormick DA (2015) Waking state: rapid variations modulate neural and behavioral responses. *Neuron* 87:1143–1161.
- Mennes M, Kelly C, Zuo XN, Di Martino A, Biswal BB, Castellanos FX, Milham MP (2010) Inter-individual differences in resting-state functional connectivity predict task-induced BOLD activity. *Neuroimage* 50:1690–1701.
- Menon V, Uddin LQ (2010) Saliency, switching, attention and control: a network model of insula function. *Brain Struct Funct* 214:655–667.
- Mesulam MM, Mufson EJ (1982) Insula of the Old World monkey: III. Efferent cortical output and comments on function. *J Comp Neurol* 212:38–52.
- Miller KJ, Leuthardt EC, Schalk G, Rao RP, Anderson NR, Moran DW, Miller JW, Ojemann JG (2007) Spectral changes in cortical surface potentials during motor movement. *J Neurosci* 27:2424–2432.
- Mittner M, Boekel W, Tucker AM, Turner BM, Heathcote A, Forstmann BU (2014) When the brain takes a break: a model-based analysis of mind wandering. *J Neurosci* 34:16286–16295.
- Moutard C, Dehaene S, Malach R (2015) Spontaneous fluctuations and non-linear ignitions: two dynamic faces of cortical recurrent loops. *Neuron* 88:194–206.
- Murphy PR, O’Connell RG, O’Sullivan M, Robertson IH, Balsters JH (2014) Pupil diameter covaries with BOLD activity in human locus ceruleus. *Hum Brain Mapp* 35:4140–4154.
- Nir Y, Mukamel R, Dinstein I, Privman E, Harel M, Fisch L, Gelbard-Sagiv H, Kipervasser S, Andelman F, Neufeld MY, Kramer U, Arieli A, Fried I, Malach R (2008) Interhemispheric correlations of slow spontaneous neuronal fluctuations revealed in human sensory cortex. *Nat Neurosci* 11:1100–1108.
- Oostenveld R, Fries P, Maris E, Schoffelen JM (2011) FieldTrip: open source software for advanced analysis of MEG, EEG, and invasive electrophysiological data. *Comput Intell Neurosci* 2011:156869.
- Oppenheimer SM, Gelb A, Girvin JP, Hachinski VC (1992) Cardiovascular effects of human insular cortex stimulation. *Neurology* 42:1727–1732.
- Papademetris X, Jackowski MP, Rajeevan N, DiStasio M, Okuda H, Constable RT, Staib LH (2006) BioImage Suite: an integrated medical image analysis suite: an update. *Insight J* 2006:209.
- Parvizi J, Kastner S (2018) Promises and limitations of human intracranial electroencephalography. *Nat Neurosci* 21:474–483.
- Reimer J, Froudarakis E, Cadwell CR, Yatsenko D, Denfield GH, Tolias AS (2014) Pupil fluctuations track fast switching of cortical states during quiet wakefulness. *Neuron* 84:355–362.
- Reimer J, McGinley MJ, Liu Y, Rodenkirch C, Wang Q, McCormick DA, Tolias AS (2016) Pupil fluctuations track rapid changes in adrenergic and cholinergic activity in cortex. *Nat Commun* 7:13289.
- Ruiz Vargas E, Soros P, Shoemaker JK, Hachinski V (2016) Human cerebral circuitry related to cardiac control: a neuroimaging meta-analysis. *Ann Neurol* 79:709–716.
- Schneider M, Hathway P, Leuchs L, Samann PG, Czisch M, Spoormaker VI (2016) Spontaneous pupil dilations during the resting state are associated with activation of the salience network. *Neuroimage* 139:189–201.
- Seeley WW, Menon V, Schatzberg AF, Keller J, Glover GH, Kenna H, Reiss AL, Greicius MD (2007) Dissociable intrinsic connectivity networks for salience processing and executive control. *J Neurosci* 27:2349–2356.
- Shine JM, Bissett PG, Bell PT, Koyejo O, Balsters JH, Gorgolewski KJ, Moodie CA, Poldrack RA (2016) The dynamics of functional brain networks: integrated network states during cognitive task performance. *Neuron* 92:544–554.
- Smallwood J, Brown KS, Tipper C, Giesbrecht B, Franklin MS, Mrazek MD, Carlson JM, Schooler JW (2011) Pupillometric evidence for the decoupling of attention from perceptual input during offline thought. *PLoS One* 6:e18298.
- Smith SM, Fox PT, Miller KL, Glahn DC, Fox PM, Mackay CE, Filippini N, Watkins KE, Toro R, Laird AR, Beckmann CF (2009) Correspondence of the brain’s functional architecture during activation and rest. *Proc Natl Acad Sci USA* 106:13040–13045.
- Stitt I, Zhou ZC, Rattke-Schuller S, Fröhlich F (2018) Arousal dependent modulation of thalamo-cortical functional interaction. *Nat Commun* 9:2455.
- Stringer C, Pachitariu M, Steinmetz N, Reddy CB, Carandini M, Harris KD (2019) Spontaneous behaviors drive multidimensional, brainwide activity. *Science* 364:255.
- Tavor I, Parker Jones O, Mars RB, Smith SM, Behrens TE, Jbabdi S (2016) Task-free MRI predicts individual differences in brain activity during task performance. *Science* 352:216–220.
- Taylor KS, Seminowicz DA, Davis KD (2009) Two systems of resting state connectivity between the insula and cingulate cortex. *Hum Brain Mapp* 30:2731–2745.
- Taylor KS, Kucyi A, Millar PJ, Murai H, Kimmerly DS, Morris BL, Bradley TD, Floras JS (2016) Association between resting-state brain functional connectivity and muscle sympathetic burst incidence. *J Neurophysiol* 115:662–673.
- Uddin LQ (2015) Salience processing and insular cortical function and dysfunction. *Nat Rev Neurosci* 16:55–61.
- Unsworth N, Robison MK (2016) Pupillary correlates of lapses of sustained attention. *Cogn Affect Behav Neurosci* 16:601–615.
- Valenza G, Sclocco R, Duggento A, Passamonti L, Napadow V, Barbieri R, Toschi N (2019) The central autonomic network at rest: uncovering functional MRI correlates of time-varying autonomic outflow. *Neuroimage* 197:383–390.
- Vogt BA, Pandya DN (1987) Cingulate cortex of the rhesus monkey: II. Cortical afferents. *J Comp Neurol* 262:271–289.
- Wang CA, Munoz DP (2014) Modulation of stimulus contrast on the human pupil orienting response. *Eur J Neurosci* 40:2822–2832.
- Wang CA, Munoz DP (2015) A circuit for pupil orienting responses: implications for cognitive modulation of pupil size. *Curr Opin Neurobiol* 33:134–140.
- Wang CA, Boehne SE, Itti L, Munoz DP (2014) Transient pupil response is modulated by contrast-based saliency. *J Neurosci* 34:408–417.
- Willenbockel V, Sadr J, Fiset D, Horne GO, Gosselin F, Tanaka JW (2010) Controlling low-level image properties: the SHINE toolbox. *Behav Res Methods* 42:671–684.
- Xiao J, Ehinger KA, Hays J, Torralba A, Oliva A (2016) Sun database: exploring a large collection of scene categories. *Int J Comput Vis* 119:3–22.
- Yellin D, Berkovich-Ohana A, Malach R (2015) Coupling between pupil fluctuations and resting-state fMRI uncovers a slow build-up of antagonistic responses in the human cortex. *Neuroimage* 106:414–427.
- Yeo BT, Krienen FM, Sepulcre J, Sabuncu MR, Lashkari D, Hollinshead M, Roffman JL, Smoller JW, Zollei L, Polimeni JR, Fischl B, Liu H, Buckner RL (2011) The organization of the human cerebral cortex estimated by intrinsic functional connectivity. *J Neurophysiol* 106:1125–1165.
- Young CB, Raz G, Everaerd D, Beckmann CF, Tendolkar I, Hendler T, Fernandez G, Hermans EJ (2017) Dynamic shifts in large-scale brain network balance as a function of arousal. *J Neurosci* 37:281–290.
- Zerbi V, Floriou-Servou A, Markicevic M, Vermeiren Y, Sturman O, Privitera M, von Ziegler J, Ferrari KD, Weber B, De Deyn PP, Wenderoth N, Bohacek J (2019) Rapid reconfiguration of the functional connectome after chemogenetic locus ceruleus activation. *Neuron* 103:702–718.e705.